Physica B 448 (2014) 199–203

Contents lists available at ScienceDirect

Physica B

journal homepage: www.elsevier.com/locate/physb

Enhanced magnetic and electrical properties of Y and Mn co-doped $BiFeO_3$ nanoparticles

A. Mukherjee [a], M. Banerjee [a], S. Basu [a,*], Nguyen Thi Kim Thanh [b], L.A.W. Green [b], M. Pal [c]

[a] Department of Physics, National Institute of Technology, Durgapur 713209, India
[b] Department of Physics and Astronomy, University College London, Gower Street, London, UK
[c] CSIR – Central Mechanical Engineering Research Institute, Durgapur, India

ARTICLE INFO

Available online 5 April 2014

Keywords:
Multiferroics
Bismuth ferrite
Nanoparticles
Magnetic properties
Electrical properties
Correlated barrier hopping

ABSTRACT

Multiferroic (Y, Mn) substituted $BiFeO_3$ had been synthesized by a facial sol–gel method. The single phase polycrystalline nature of samples was confirmed from X-ray diffraction pattern. The average particle size was estimated to be around 30–32 nm from transmission electron microscopy. The magnetic properties of codoped nanoparticles had been studied using Bloch equation and the estimated value of the Bloch constant was found to be much larger than usual ferromagnetic materials. Coercivity values for different temperature is used to calculate the blocking temperature and found to lie above room temperature. The dc electrical transport properties were studied in the temperature range 298– 523 K and explained using a Motts 3D variable range hopping model and the density of states was estimated near the Fermi level. The ac electrical data were found to follow the correlated barrier hopping model. Well-developed *PE* hysteresis loops were observed in codoped nanoparticles, which were attributed to a decrease in oxygen vacancies, bismuth volatisation due to doping and an increase of the effective potential barrier height for charge carriers.

© 2014 Elsevier B.V. All rights reserved.

1. Introduction

Bismuth ferrite (BFO) is one of the promising room temperature multiferroic materials which show ferroelectric ordering below Curie temperature (1103 K) and space-incommensurate antiferromagnetism below the Néel temperature (643 K) and enable a coupling interaction between ferroelectric and antiferromagnetic order. This kind of coupling interaction also called the magnetoelectric coupling produces mutual control and detection of electrical polarization and magnetism [1,2]. Upon extensive research in the past few years, it was confirmed that multiferroic properties of BFO can be greatly tailored toward an ideal multiferroic material through suitable doping [3–6] and/or forming solid-state-solution with other perovskite type oxides [7]. Several groups tried to improve the magnetic properties of BFO by suitably doping with rare earth elements like La^{3+}, Nd^{3+}, Gd^{3+}, Sm^{3+}, Pr^{4+} [8–11] where the dopants produce magnetization by suppressing the spiral spin structure of BFO. Several groups also tried to improve the ferroelectrical, electrical and optical properties of BFO by doping strategies [12–15]. However co-doping is a much more efficient way to tailor the magnetoelectric properties of BFO. Local ferrimagnetic/ferromagnetic structure for improving the magnetic moment in bismuth ferrite has been proposed in transition metal doped $Bi_{0.8}La_{0.2}Nb_{0.01}Fe_{0.94}TR_{0.05}O_3$ [16]. Several groups have attempted to ameliorate the electrical and magnetic properties of BFO by virtue of codoping [17–19]. In this paper we report the detailed magnetic and electrical properties of Y–Mn codoped BFO explaining some theoretical models which are useful in device applications.

2. Experimental

2.1. Material and methods

Codoped $BiFeO_3$ ($Bi_{1-x}Y_xFe_{1-y}Mn_yO_3$) ($x=0.01$, $y=0.01$, 0.05) nanoparticles designated as $BiFeO_3$ (Pure), $Bi_{0.99}Y_{0.01}FeO_3$ (1Y), $BiFe_{0.99}Mn_{0.01}O_3$ (1Mn), $Bi_{0.99}Y_{0.01}Fe_{0.99}Mn_{0.01}O_3$ (1Y–1Mn), $Bi_{0.99}Y_{0.01}Fe_{0.95}Mn_{0.05}O_3$ (1Y–5Mn) were prepared by a simple sol–gel route. Weighted amounts of Bi $(NO_3)_3\cdot 5H_2O$ (Sigma-Aldrich, 99.99%), Fe $(NO_3)_3\cdot 9H_2O$ (Sigma-Aldrich, 98%+), Y $(NO_3)_3.10H_2O$ (Sigma Aldrich, 99.99%) and $Mn(NO_3)_2\cdot 4H_2O$ (Alfa Aesar, 99.9%) were dissolved in 20 ml distilled water under continuous stirring. The reaction medium was made acidic by using HNO_3 and pH of the solution was maintained at 2. In the next step, 0.03 mol of malic acid was dissolved in 30 ml distilled water in a separate beaker.

* Corresponding author. Tel.: +91 343 254 6808.
E-mail address: soumen.basu@phy.nitdgp.ac.in (S. Basu).

http://dx.doi.org/10.1016/j.physb.2014.03.082
0921-4526/© 2014 Elsevier B.V. All rights reserved.

Metal nitrate precursor solutions were added to malic acid under continuous ultrasonication. Polyethylene glycol (PEG) and malic acid in a molar ratio of 1:1 were subsequently added to the solution as a capping agent. The solution was dried to get precursor powder. Finally the ground powders were calcined in air at 873 K for 2 h.

2.2. Characterization

The single phase formation of ($Bi_{1-x}Y_xFe_{1-y}Mn_yO_3$) ($x=0.01$, $y=0.01$, 0.05) nanocrystals was confirmed by X-ray diffraction pattern. X-ray diffraction of these samples was recorded by an X'Pert Pro X-ray diffractometer (Panlytical, Almelo, Netherlands) fitted with nickel-filtered Cu Kα radiation ($\lambda=1.5414$ Å) in 2θ range from 20° to 80°. The transmission electron microscope (HRTEM, JEOL 2011) study confirmed the size and formation of BFO and co- doped BFO nanoparticles. The magnetic properties of the samples were measured by using a superconducting interface device (SQUID) magnetometer MPMS (Quantum Design, USA) fitted with a 7 T magnet. For electrical measurements the powder was taken in a steel mold of 1 cm diameter and compacted at a pressure of 7 t/cm^2. Silver paint electrodes (supplied by Acheson Colloiden. B.V. Holland) were applied on two opposite faces. Direct-current (dc) conductivity was measured by using Keithley 6514 electrometer. The temperature dependence of conductivity was measured in a furnace fitted with a Eurotherm temperature controller. The ac measurement was performed using an Agilent E4980A LCR meter. Room temperature ferroelectric loops were studied using a Radiant Technology precision premier II workstation (USA).

3. Result and discussions

XRD patterns of codoped BFO nanoparticles calcined at 873 K are presented in Fig. 1. All the prominent peaks in the plot are indexed to various ($h\,k\,l$) planes of $BiFeO_3$ (JCPDS no. 86-1518), demonstrating the formation of single phase $BiFeO_3$ nanoparticles. The transmission electron microscopy study was done to estimate the average particles size and is found to be in the range of 30–32 nm. Fig. 2(a) shows a typical TEM image of the 1Y–1Mn sample. Fig. 2 (b) shows the high resolution TEM image of 1Y–1Mn sample taken from a portion of Fig. 2(a). The lattice planes (0 1 2) and (0 2 4) are clearly observed and match well with JCPDS no. 86-1518 confirming the good crystalline nature of BFO. Fig. 2(c) shows the SAED pattern taken from Fig. 2(a), which also reconfirmed the formation of BFO.

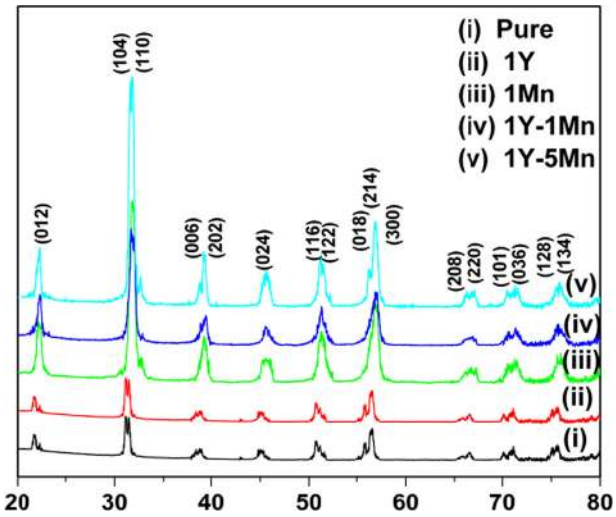

Fig. 1. X-ray diffraction pattern for all samples.

Fig. 2(d) shows the EDS spectrum, taken from a portion of Fig. 2(a), which again confirms the presence of all the elements of 1Y–1Mn nanoparticles.

The hysteresis loop at 300 K for all the samples presented in Fig. 3(a and b) shows the enlarged view of Fig. 3(a) in the lower field region. Shapes of the curves confirm the ferro/ferrimagnetic nature of the samples. The magnetisation behavior of the samples had been analysed on the basis of Bloch function [20,21] given by

$$M_S(T) = M_S(0)[1 - BT^{3/2}] \quad (1)$$

where $M_s(T)$ and $M_s(0)$ are the saturation magnetizations at temperatures T K and 0 K, respectively, and B is the Bloch constant. Fig. 3(c) shows the variation of $M_s(T)$ with $T^{3/2}$. It is clearly observed that saturation magnetization is increased with doping and it has taken maximum value in the case of 1Y–1Mn. We have fitted M_s (T) experimental data to Eq. (1) using M_s (0) and B as parameters. The value of Bloch constant is estimated to be 4×10^{-5} K$^{-3/2}$ which is much larger than ferromagnetic metals like α-Fe [22] and $YFeO_3$ [23]. Bulk perovskite BFO is antiferromagnetic ($T_N \approx \approx 643$ K) in nature and exhibits very weak magnetization at room temperature due to a residual moment from a canted spin structure. BFO nanoparticles show ferromagnetic-like behavior due to the breakdown periodicity of the spin cycloid of iron. The potential causes for the increase in macroscopic magnetization were the suppressed inhomogeneous magnetic spin structure, increased canting angle due to co-doping and the formation of Fe^{+2} ions. However it is well established that during high temperature annealing process, coexistence of Fe^{+2} and Fe^{+3} is unavoidable [24]. The existence of Fe^{+2} ions would possibly cause a double exchange interaction between Fe^{+2} and Fe^{+3} ions through oxygen which may result in the enhancement of ferromagnetism [25,26]. When Mn is the only dopant, the magnetization increases due to the magnetic moment of Mn itself and the charge compensation effect. In case of 1Y–1Mn the pop-in of Y conflicted with Mn and pinned the Mn valance state. Y makes an impact on Fe and the moment of Mn can help strengthen the magnetization together with Fe valance state variation and Fe^{+2}–O–Fe^{+3} superexchange interaction caused by Y doping. However the potential cause for the decrease of magnetization in 1Y–5Mn is the structural distortion.

The variation of coercivity H_c with temperature for different samples is displayed in Fig. 3(d). The large value of coercivity observed indicates that the samples are not superparamagnetic below the room temperature. It is evident from Fig. 3(d) that the coercivity value increases as the temperature is lowered. This is to be expected in the case of ferro/ferrimagnetic particles [16]. The thermal dependence of H_c is expected to follow the equation

$$H_c = H_c(0)\lfloor 1 - A(T)^k \rfloor \quad (2)$$

where H_c (0) is the coercive field at $T=0$ K, and A and k are the parameters given by the following relation:

$$A = [\beta k_B / VK_{eff}]^k \quad (3)$$

where k_B is Boltzmann constant, $\beta=\ln(\tau_m/\tau_0)$ depends on the typical measuring time τ_m and characteristic time τ_0 and $K_{eff}=K_V+(6/d)\,K_S$, is the effective anisotropy constant, where K_V is the bulk anisotropy energy per unit volume, K_S is the surface density of anisotropy energy and d is the diameter of the particle [20]. It has been shown that a perfect spherical particle should have a zero net contribution from surface anisotropy and the exponent k has a value of 0.5 for an assembly of aligned particles [21] and $k=0.77$ for randomly oriented particles [22]. Again from Arrhenius–Néel relation [23] the blocking temperature is given by

$$T_B = \frac{VK_{eff}}{\beta k_B} \quad (4)$$

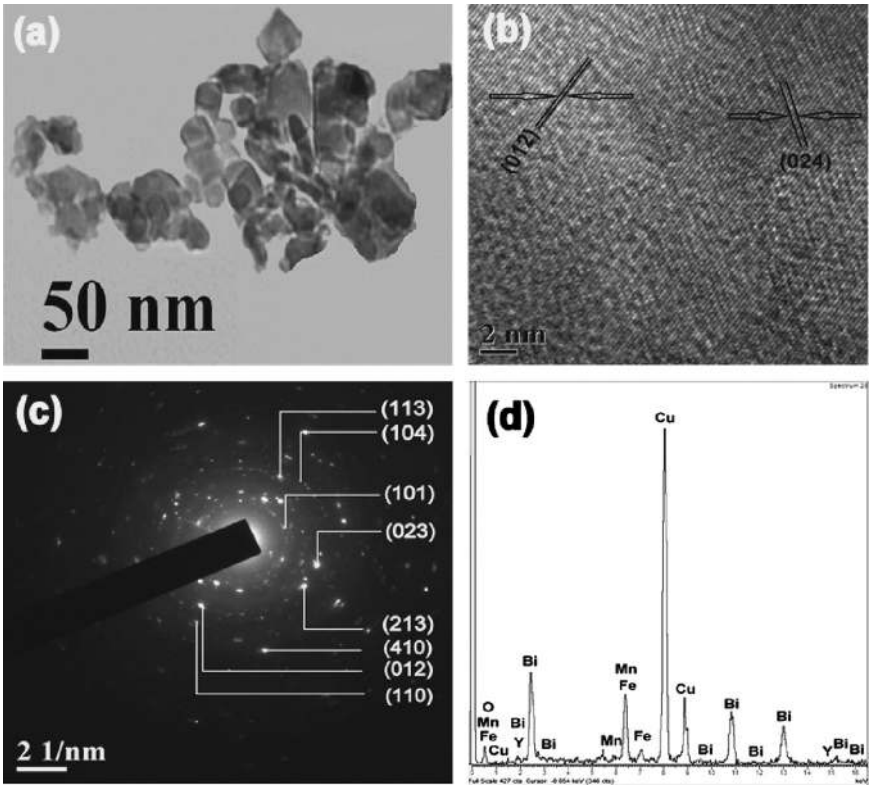

Fig. 2. (a) TEM image of 1Y–1Mn sample; (b) HRTEM image taken from a portion of (a); (c) SAED pattern taken from a portion of (a); and (d) EDS pattern taken from a portion of (a).

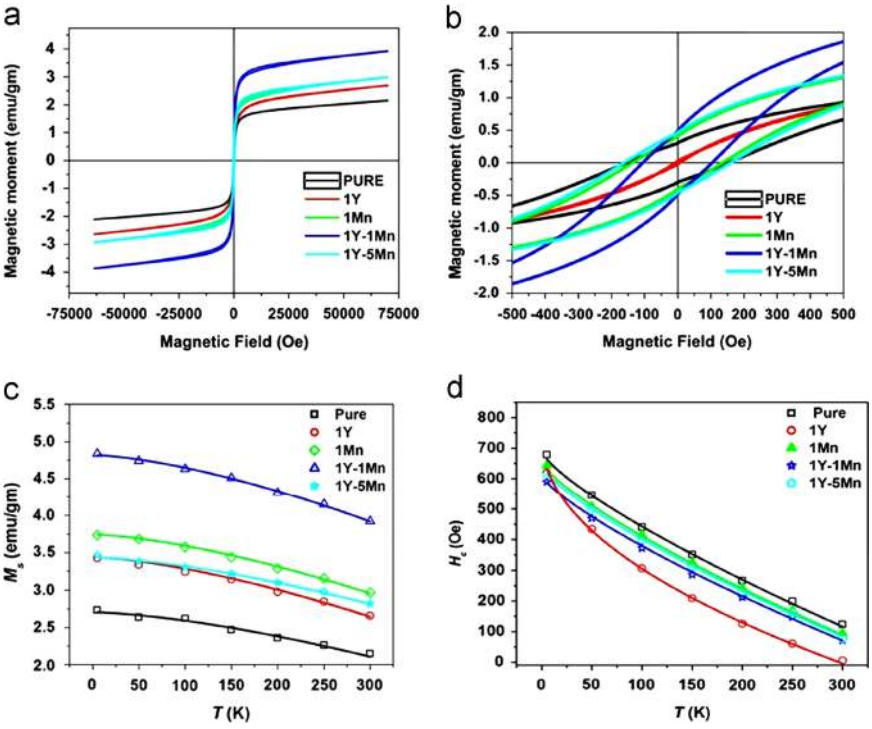

Fig. 3. (a) Room temperature hysteresis loop for all the samples; (b) enlarged view of (a) for better clarity; (c) variation of M_s (T) with $T^{3/2}$; and (d) variation of coercivity H_c with temperature for different samples.

We have fitted H_c (T) experimental data in Eqs. (2) and (4) using H_c (0) and T_B as parameters. The value of k is taken as 0.77. Values of estimated blocking temperatures are summarised in Table 1. It was clearly observed that the estimated blocking temperature for all samples remain above room temperature which again confirmed the ferro/ferromagnetic nature of the codoped samples at room temperature. This enhances the application potentiality of codoped BFO in magnetic sensor devices.

The dc and ac conduction mechanisms had been observed in the temperature range 298–523 K and in the frequency range

20 Hz–1 MHz. It is evident from the figure that, with the increase of doping, there is an increase in the resistivity of the samples by a significant amount and decreases the leakage current which is essential for device application. In order to explain the dc conduction mechanism the data for all the samples were analyzed by Mott's variable range hopping model, [27]. According to this model the resistivity is given by

$$\rho = \rho_0 \exp\left(\frac{T}{T_0}\right)^{1/4} \tag{5}$$

$$T_0 = 2.1\left[\frac{\alpha^3}{k_B N(E_F)}\right] \tag{6}$$

where α^3 is the localization length describing the localized state, $N(E_F)$ is the density of states near the Fermi level, and k_B is the Boltzmann constant. Fig. 4(a) gives the resistivity variation as a function of $T^{-1/4}$. The points represent the experimental data and the lines are the theoretical fits. In order to estimate the value of $N(E_F)$, we have chosen a reasonable value of α as 0.12 $Å^{-1}$ [27] and then calculated $N(E_F)$ from the slope of the line in Fig. 4(a) using Eq. (5).The values of the density of states $N(E_F)$ as extracted from this fitting are summarized in Table 1.

The alternating current (ac) conductivity of the codoped bismuth ferrite nanoparticles has been measured in the temperature range 298 K ≤ T ≤ 523 K and frequency range 20 Hz–1 MHz. At a lower range, the conductivity is almost frequency independent but becomes predominant at higher range for a particular temperature. In general many nanocrystalline systems have dc conductivity contribution (σ_{dc}) besides the ac conductivity. This may be the reason behind the frequency independence of conductivity at lower frequency region. The total conductivity at a particular temperature over a wide range of frequency obeys a power law with frequency, which can be expressed as [28–31]

$$\sigma'(f) = \sigma_{dc} + \sigma_{ac}(f) = \sigma_{dc} + \alpha f^S \tag{7}$$

where σ_{dc} is the dc conductivity, α is the temperature dependent constant and the frequency exponent $S \leq 1$. The frequency dependent contribution can be calculated by subtracting the dc contribution from the total conductivity. This linear variation of ln $[\sigma_{ac}(f)]$ with ln[f] shows that the frequency exponent 'S' in Eq. (7), is independent of frequency. The variation of 'S' with temperature for different samples is shown in Fig. 4(b). A gradual decrease of 'S' with increasing temperature is elucidated by considering the correlated barrier hopping (CBH) model. According to CBH model, the value of 'S' decreases gradually with increase of temperature. The nature of variation of 'S' in the present study samples suggests that the CBH model is suitable for explaining the experimental data. According to this model, the charge carriers hopp between the sites over the potential barrier separating them and the frequency exponent 'S' can be expressed as [29]

$$S = 1 - \frac{6k_BT}{W_H - k_BT\, In(1/\omega\tau_0)} \tag{8}$$

where k_B, W_H, ω and τ_0 are Boltzmann constant, effective barrier height, angular frequency and characteristic relaxation time, respectively.

Thus, the experimental data has been analyzed with Eq. (8) as function of temperature keeping W_H and $\omega\tau_0$ as fitting parameters in Fig. 4(b). The points indicate the experimental data and solid lines give the theoretical best fit obtained from Eq. (8) for different samples. The values of W_H and τ_0 have been calculated at a fixed frequency of 10 kHz and are enlisted in Table 1.

Fig. 5(a) shows the room temperature polarization vs electric field (P–E) curves for the pure and doped BFO samples measured at a frequency of 50 Hz. All figures clearly demonstrate that well saturated hysteresis loops are observed with applied electric fields up to 2000 V/cm. Generally, it is difficult to measure the stable P–E curves of the BFO at room temperature in the high electric field region as breakdown occurs because of large leakage current. This improvement in ferroelectric-behavior in codoped samples might be attributed to the reduction of charge defects like oxygen vacancies (which plays a crucial role in the pinning of polarization switching domain) [31–34] and bismuth vacancies as they originate from bismuth volatization and transition from Fe^{+3} to Fe^{+2} as shown in the equation below

$$4Bi^{3+} + 6O^{2-} \rightarrow 4Bi\ (gas) + 3O_2\ (gas) + 4V_{Bi}^{3-} + 6V_O^{2+}$$

$$4Fe^{3+} + 2O^{2-} \rightarrow 4Fe^{2+} + O_2\ (gas) + 2V_O^{2+}$$

Incorporation of yttrium ions in the bismuth site helps to reduce the bismuth volatization and oxygen vacancies. Fig. 5(b) displays the frequency profile of 1Y–1Mn sample at room temperature. It was observed that frequency dependence of E_c is not pronounced, however, with increase in frequency the value of remnant polarization decreases continuously due to leakage current and non-linear dielectric effects. Well saturated PE hysteresis loops for 1Y–1Mn sample under the application of electric field of different amplitudes are shown in Fig. 5(c) for more clarity.

Table 1
A comparison between different parameters obtained from magnetic and electrical measurements (both ac and dc).

Sample	T_B (K)	W_H (eV)	τ_0 (S)	$N(E_F)$(eV^{-1} cm^{-3})
Pure	367	4.32	1.19×10^{-12}	1.33×10^{22}
1Y	365	4.08	9.59×10^{-14}	5.33×10^{22}
1Mn	359	3.60	1.8×10^{-13}	8.22×10^{20}
1Y–1Mn	361	4.05	1.56×10^{-11}	3.65×10^{20}
1Y–5Mn	351	3.56	4.8×10^{-13}	6.47×10^{20}

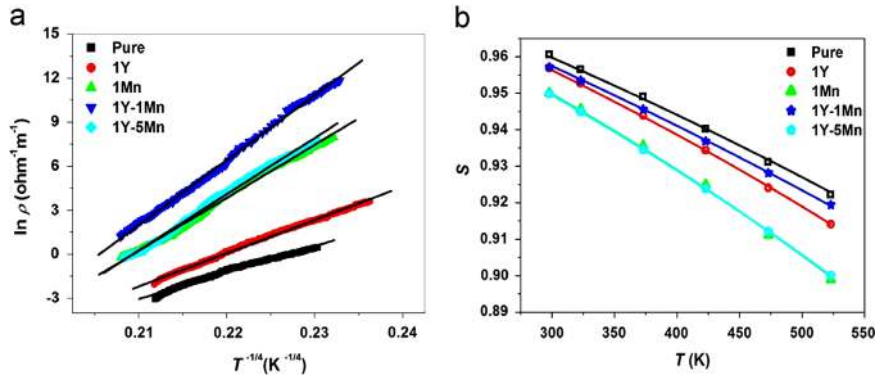

Fig. 4. (a) Variation of resistivity with temperature and (b) variation of 'S' with temperature for different samples.

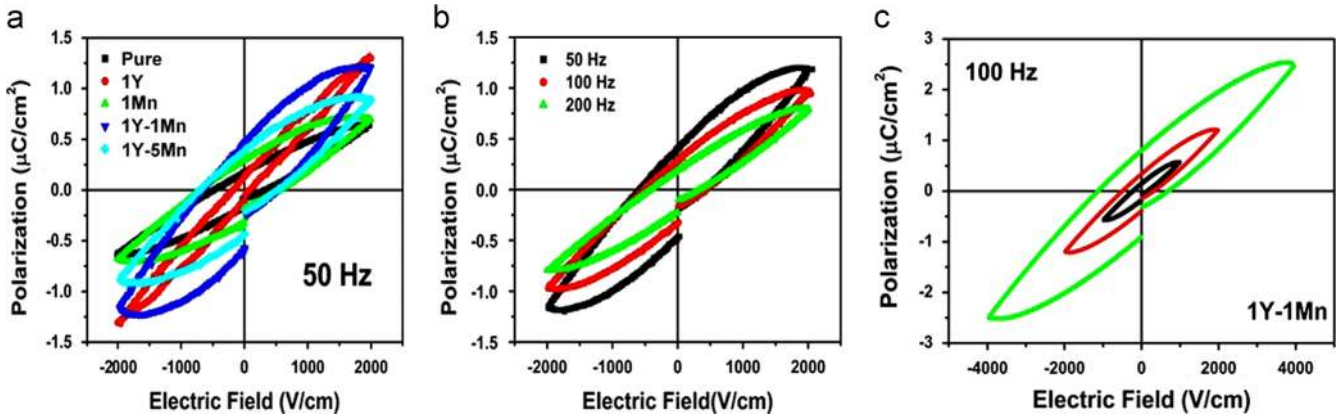

Fig. 5. (a) *PE* loops for all samples at 50 Hz; (b) *PE* loop for 1Y–1Mn sample at different frequenciesand (c) *PE* loop for 1Y–1Mn at different electric field at 100 Hz.

4. Conclusion

Multiferroic bismuth ferrite pure and codoped with average particle size of around 30–32 nm had been synthesized by a simple sol–gel route. Its magnetic properties were studied in detail using conventional theoretical models. The saturation magnetization satisfies the Bloch relation and the Bloch constant was estimated to be much higher than ferromagnetic metals like α-Fe and $YFeO_3$. Coercivity values show that the samples are superparamagnetic up to room temperature. Blocking temperature of the samples had been estimated from the thermal dependence of coercivity. The dc conduction mechanism shows that the sample shows variable range hopping mechanism and the density of states was calculated. We explain the ac conductivity results by considering the correlated barrier hopping (CBH) model and calculated the effective barrier height and characterization relaxation time. Stable room temperature polarization versus electric field (*P*–*E*) curves for the pure and codoped BFO samples had been measured at a frequency of 50 Hz. The improvement in ferroelectric behavior is attributed to the reduction of charge defects like oxygen vacancies and bismuth vacancies.

Acknowledgment

The authors would like to acknowledge financial support from the Board of Research in Nuclear Science (BRNS) (Project no. 2011/37P/14/BRNS), Government of India. The authors also acknowledge the Centre of Excellence in Advanced Material, NIT Durgapur. The authors would also like to thank Department of Science and Technology (DST) (SR/FTP/PS-66/2008), Government of India for providing financial assistance. Ayan Mukherjee thanks Council for Scientific and Industrial Research for his Senior Research Fellowship.

References

[1] M. Fiebig, J. Phys. D: Appl. Phys. 38 (2005) R123.
[2] Z.X. Cheng, X.L. Wang, K. Ozawa, H. Kimura, Appl. Phys. Lett. 40 (2007) 703.
[3] A. Mukherjee, M. Banerjee, S. Basu, P.M. G. Nambissan, M. Pal, J. Phys. D: Appl. Phys. 46 (2013) 495309.
[4] A. Mukherjee, S. Basu, G. Chakraborty, M. Pal, J. Appl. Phys. 112 (2012) 014321.
[5] G.L. Yuan, S.W. Or, J.M. Liu, Z.G. Liu, Appl. Phys. Lett. 89 (2006) 052905.
[6] C.-H. Yang, J. Seidel, S.Y. Kim, P.B. Rossen, P. Yu, M. Gajek, Y.H. Chu, L.W. Martin, M.B. Holcomb, Q. He, P. Maksymovych, N. Balke, S.V. Kalinin, A.P. Baddorf, S. R. Basu, M.L. Scullin, R. Ramesh, Nat. Mater. 8 (2009) 485.
[7] T. Kanai, S.I. Ohkoshi, A. Nakajima, T Watanabe, K. Hashimoto, Adv. Mater. 13 (2001) 487.
[8] S.T. Zhang, Y. Zhang, M.H. Lu, C.L. Du, Y.F. Chen, Z.G. Liu, Y.Y. Zhu, N.B. Ming, X. Q. Pan, Appl. Phys. Lett. 88 (2006) 162901.
[9] F.Z. Huang, X.M. Lu, W.W. Lin, X.M. Wu, Y. Kan, J.S. Zhu, Appl. Phys. Lett. 89 (2006) 242914.
[10] V.A. Khomchenko, D.A. Kiselev, I.K. Bdikin, V.V. Shvartsman, P. Borisov, W. Kleemann, J.M. Vieira, A.L. Kholkin, Appl. Phys. Lett. 93 (2008) 262905.
[11] F. Yu, M.Y. Li, Z.Q. Hu, L. Pei, D.Y. Guo, X.Z. Zhao, S.X. Dong, Appl. Phys. Lett. 93 (2008) 182909.
[12] G. L Yuan, Or.S Wing, J. Appl. Phys. 100 (2006) 024109.
[13] Sk. M. Hossain, A. Mukherjee, S. Chakraborty, S.M. Yusuf, S. Basu, M. Pal, Mater. Focus 2 (2013) 1.
[14] A. Mukherjee, Sk. M. Hossain, S. Basu, M. Pal, Appl. Nanosci. 2 (2012) 305.
[15] Sk. M. Hossain, A. Mukherjee, S. Basu, M. Pal, Micro Nano Lett. 8 (2013) 374.
[16] Z X Cheng, X L Wang, Y Du, S X Dou, J. Phys. D: Appl. Phys. 43 (2010) 242001.
[17] J. Silva, A. Reyes, R. Castañeda, H. Esparza, H. Camacho, J. Matutes, L. Fuentes, Ferroelectrics 426 (2012) 103.
[18] N. Adhlakha, K.L. Yadav, R. Singh, Sci. Adv. Mater. 5 (2013) 947.
[19] X. Zheng, Q. Xu, Z. Wen, X. Lang, D. Wu, T. Qiu, M.X. Xu, J. Alloys Compds. 499 (2010) 108–112.
[20] F. Bloch, Z. Phys. A 61 (1930) 206.
[21] D. Zhang, K.J. Klabunde, C.M. Sorensen, Phys. Rev. B 58 (1998) 14167.
[22] S. Mathur, M. Veith, R. Rapalaviciute, H. Shen, G.F. Goya, W.L. Martins Filho, T.S. Berquo, Chem. Mater. 16 (2004) 1906.
[23] R.P Maiti, S. Basu, D. Chakravorty, J. Magn. Magn. Mater. 321 (2009) 3274.
[24] Y. Wang, Q.H. Jiang, H.C. He, C.W. Nan, Appl. Phys. Lett. 88 (2006) 142503.
[25] J. Wang, A. Scholl, H. Zheng, S.B. Ogale, D. Viehland, D.G. Schlom, N.A. Spaldin, K.M. Rabe, M. Wuttig, L. Mohaddes, J. Neaton, U. Waghmare, T. Zhao, R. Ramesh, Science 307 (2005) 1203b.
[26] F. Huang, X. Lu, W. Lin, X. Wu, Y. Kan, J. Zhu, Appl. Phys. Lett. 89 (2006) 242914.
[27] N.F. Mott, Philos. Mag. 19 (1969) 835.
[28] N.F. Mott, E. Davis, Electronic Process in Noncrystalline Materials, 2nd ed., Clarendon Press, Oxford, 1979.
[29] S.R. Elliott, Adv. Phys 36 (1987) 135.
[30] A.L. Efros, Philos. Mag. B 43 (1981) 829.
[31] A.R. Long, Adv. Phys. 31 (1982) 553.
[32] X.D. Qi, J Dho, R. Tomov, M.G. Blamire, J.L. MacManus-Driscoll, Appl. Phys. Lett. 86 (2006) 062903.
[33] H. Uchida, I. Okada, H. Matsuda, T. Iijima, T. Watanabe, H. Funakubo, Jpn. J. Appl. Phys. 43 (2005) 2636.
[34] J.K. Kim, S.S. Kim, W.J. Kim, Mater. Lett. 59 (2005) 4006.